High-precision astrometric measurements of calibration satellites

Jovan Skuljan
Defence Technology Agency, Auckland, New Zealand

ABSTRACT

The Defence Technology Agency (DTA) of the New Zealand Defence Force (NZDF) operates a space domain awareness (SDA) observatory located at Whangaparaoa peninsula just north of Auckland, New Zealand. The observatory is equipped with two 28-cm telescopes mounted side-by-side on a Paramount ME II robotic tracking mount. A range of cooled CCD cameras are used for imaging, and a specialized global positioning system (GPS) unit was developed for accurate timing.

Over the past several years, the observation program of the DTA observatory consisted of astrometric, photometric and polarimetric measurements of satellites in all orbital regimes. More recently, the focus had shifted to high-precision astrometric measurements of calibration satellites, mainly in geostationary Earth orbit (GEO) and medium earth orbit (MEO). It was demonstrated that small-aperture equipment can be used for obtaining astrometric data of high precision (low random error) and high accuracy (low systematic error). However, special attention must be paid to the image analysis and data reduction process. We have achieved this in-house by creating a dedicated SDA data analysis tool, StarView, optimised for images obtained with the DTA equipment.

The astrometric calibration in StarView is based on the European Space Agency's (ESA) GAIA catalogue (Data Release DR-2). For practical purposes, the catalogue was limited down to magnitude 16, in order to keep the total number of stars manageable, while providing enough data for reliable calibration. For the recognition of a stellar field and identification of individual stars in the image, we use our own algorithm called stellar fingerprints. After several years of application, this method proved to be extremely fast and reliable. The average random uncertainty of a typical astrometric solution is about 0.2 arc seconds, based on several hundred stars within the field of view.

In addition to the stellar fingerprint algorithm, which is only used on frames in sidereal mode, i.e. when the stars appear as point sources, a different technique is used when tracking a satellite, and stars leave traces. Instead of analysing each stellar trace, which can be difficult for faint objects, StarView applies a two-dimensional cross-correlation between the satellite image and the star catalogue to determine the shift in right ascension and declination. This ensures that every star in the image makes a contribution to the overall cross-correlation profile. The random errors in satellite astrometry are typically very low, between 0.2 and 0.5 arc seconds, depending on the image quality.

A number of observations of calibration satellites were made in order to test the accuracy of our measurements. The astrometric coordinates were compared with the calibration ephemeris data provided by the 18th Space Defense Squadron (18 SDS) in Vandenberg, CA. The residuals showed a low scatter comparable with the random measurement errors, typically within a fraction of an arc second.

1. INTRODUCTION

Over the past several years, there has been a steady growth in the Space Domain Awareness (SDA) capability within the Defence Technology Agency (DTA) of the New Zealand Defence Force (NZDF). As a result, a fully automated and remotely operated optical observatory, named Ruru (Māori name for a native owl), has been constructed to enable satellite tracking in all orbital regimes. The observatory is located at the tip of Whangaparaoa Peninsula, about 50 km north of central Auckland. The site provides reasonably dark skies, with most of the light pollution caused by the Auckland city lights concentrated towards the south (i.e. in the direction of the celestial pole). This is usually not a concern, as the observations are mainly made around the equatorial belt, towards the north.

Since 2018, the main focus of observations made from the DTA Ruru SDA Observatory was on certain targets of interest in the Geostationary Earth Orbit (GEO). This included both astrometric (position) and photometric (brightness) measurements in collaboration with our overseas partners [1]. More recently, in 2020 and 2021, the DTA made a contribution to the five-nation SDA experiment called "Phantom Echoes" [2,3], focusing on the

rendezvous and proximity operations in GEO. A number of observations were made of the Mission Extension Vehicles 1 and 2 (MEV-1, MEV-2) operated by Northrop Grumman. In particular, the MEV-1 operation took place over the Western Pacific, in clear view from New Zealand, and observations were made of the final approach between MEV-1 and Intelsat 901, just hours before the docking [4].

As part of the Phantom Echoes experiment, special attention was placed on sensor calibration in order to enable the data sharing between the participants. This was done by making observations of selected calibration satellites and sending the data for assessment to the US Space Force, 18th Space Defense Squadron (18 SDS) based in Vandenberg, California. More recently, the DTA was given access to the reference ephemeris files for selected satellites, which has enabled a direct comparison between the observations and the ephemeris data. Some of these results are presented in this paper.

2. OBSERVATIONS

A number of observations were made of two Tracking and Data Relay Satellites (TDRS) in GEO over three observation nights in August 2022, as summarised in Table 1 below.

Table 1. Observation list

Target	Date	UTC Start	UTC End	Duration	Number of Images
TDRS 10	1-Aug-2022	6:46	10:37	$3^h\ 51^m$	569
TDRS 11	3-Aug-2022	6:51	10:53	$4^h\ 02^m$	608
TDRS 10	4-Aug-2022	6:56	10:28	$3^h\ 32^m$	554

The observations were made using the Celestron EdgeHD 11 Schmidt–Cassegrain telescope of the DTA Ruru Observatory. The telescope has an aperture of 279 mm and a focal length of 2800 mm (focal ratio f/10). As a detector, a Finger Lakes Instrumentation (FLI) MicroLine ML11002 camera was used. The camera has a full-frame (36 × 24 mm) sensor with a resolution of 4008 × 2672 pixels, and a pixel size of 9 µm. This gives an image scale of about 0.66 arc seconds per pixel, suitable for high-resolution astrometric work. A specialised GPS unit was also built for accurate timing of exposures to within 1 ms based on the shutter signals generated by the camera.

All images were taken with a 5-second exposure while tracking the satellite. The detection limit at this exposure duration was about magnitude 15. On the other hand, the brightness of the satellite was typically about magnitude 12 at the start of the observation sequence, and reaching magnitude 10 towards the end. The sampling rate was about three frames per minute. Occasional interruptions in the observation sequence were made to refocus the telescope and reacquire the target.

In addition to the satellite images described above, a number of reference stellar frames were taken using 10-second exposures. The stellar images were required for the initial astrometric calibration, as explained in the next section. Also, as a standard procedure, a series of dark frames were taken on each observation night, and a median dark was subtracted from all images during the data reduction.

3. DATA REDUCTION

All data reductions presented in this paper were performed using StarView, a software tool developed at DTA for the analysis of SDA images [5]. As of 2018, the software now includes a database of about one million stars down to magnitude 16 from the GAIA DR-2 catalogue [6] by the European Space Agency (ESA).

3.1 Reduction of stellar images

A typical reduction procedure starts with a single stellar image which is used for a reference astrometric solution. As a result, a set of parameters are obtained to enable the transformation between the pixels in the image and coordinates in the sky. The astrometric solution is in a form of a two-dimensional polynomial fit, where the free

term defines the offset of the image in the sky, i.e. the equatorial coordinates of the image centre, while the higher-order terms describe the orientation and pixel scale. As the telescope moves between different parts of the sky, only the free term changes, while the overall shape of the astrometric solution remains the same (assuming that the telescope is on an equatorial mount). This is used in StarView for the calibration of satellite images, when only the free term of the solution is determined from the stellar traces found in the field of view (see Section 3.2 below). It is therefore essential that the reference astrometric solution is of the highest quality. For example, the stellar frames taken on the three observation nights listed in Table 1 were of moderately crowded fields close to the Milky Way and containing over 1000 stars suitable for the calibration.

The core engine of the astrometric calibration in StarView is a highly efficient algorithm developed at DTA for the identification of the sky region called "stellar fingerprints". The algorithm was first introduced in 2016 for the analysis of wide-field images (25 – 60 degrees) taken with conventional lenses [5]. It was subsequently modified to be used with narrow-field images (1 – 4 degrees) taken with the DTA telescopes. The main idea behind stellar fingerprints is illustrated in Fig. 1, previously published in [5].

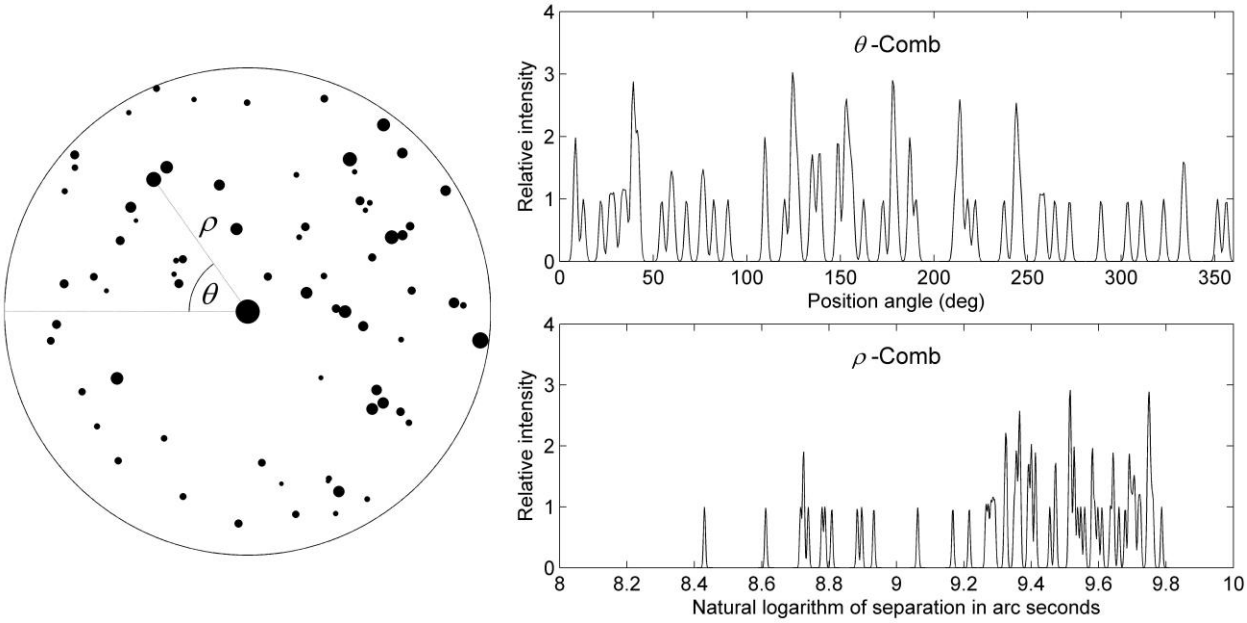

Fig. 1. Stellar fingerprints

A single stellar fingerprint is a small circular field of a given radius around a central star. The field stars found inside the circle define the fingerprint by their position in polar coordinates (ρ, θ). Thousands of fingerprints are stored in a database, and a stellar image is compared with each fingerprint until a match is found. However, to make this process efficient, the fingerprints are not stored as two-dimensional images, but rather as two separate one-dimensional images called "combs", which resemble emission line spectra. The θ-comb contains a peak at every position angle where a field star is found. When there are two or more stars sharing the same position angle, the peaks in the "spectrum" appear stronger. When the image is rotated, the θ-comb is shifted, but the relative positions of the peaks do not change. Similarly, the ρ-comb contains a peak at every radius where a field star is found. The scale is now logarithmic, so that when the image radius is changed (e.g. for an image taken at a different pixel scale), the entire "spectrum" is shifted, but the relative spacing remains the same. As a result of this arrangement, the process of comparing a stellar image with a given fingerprint consists of two separate one-dimensional cross-correlations between the image combs and the fingerprint combs. The cross correlation in θ gives the best rotation angle to match the fingerprint, while the cross-correlation in ρ gives the best image scale. As a final check, the transformed star pattern is compared with the set of stars detected in the image, and if the star positions do not match, then the next stellar fingerprint is examined.

In its original application on wide-field images, the algorithm did not require any assumptions about the telescope position. The stellar fingerprints were based on the Hipparcos catalogue [7] and only the brightest stars were used, so the fingerprints for the entire sky could easily be stored in the database. However, with the increased number of stars in the GAIA catalogue required for the calibration of narrow-field images, it was found that the telescope position needs to be used to generate a temporary database of the fingerprints in the surrounding parts of the sky. The temporary database remains in storage as long as the stellar images are within the same region.

The stellar fingerprint algorithm described above is only used to identify a small central part of a stellar image, containing perhaps a few dozen stars. This provides an initial polynomial fit which is then used to identify the remaining stars in the field of view. A final astrometric solution based on several hundred (sometimes over a thousand) stars gives a typical root mean square (RMS) error of about 0.2 arc seconds.

3.2 Reduction of satellite images

A typical satellite image contains a single point source of light close to the middle of the frame, and multiple stellar traces produced by all the stars passing through the field of view during the exposure. All stellar traces are of the same length and are parallel to each other. The orientation and length of the stellar traces are determined by the direction and speed of the telescope motion while tracking the satellite. A typical satellite image is shown in the left panel of Fig. 2 below.

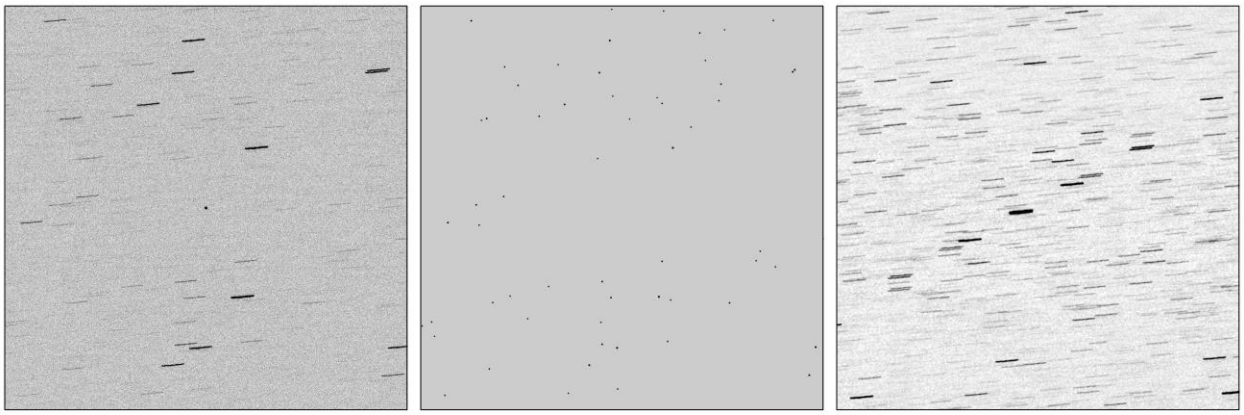

Fig. 2. Left: Observed satellite image. Centre: Simulated stellar image. Right: Cross-correlation image.

In order to derive the equatorial coordinates of the satellite in a given image, a local astrometric solution for that frame needs to be determined, based on the stars found in the same field of view. Although this is very similar to the problem of astrometric calibration on a stellar frame described above, the satellite image does not show stars as point sources. A special algorithm would be required for the extraction and measurement of each stellar trace in order to find the exact centre of the profile corresponding to the middle of the exposure. This can be done relatively easily on brighter stellar traces, but the measurement becomes increasingly more difficult for fainter stars. Furthermore, a stellar trace is intrinsically fainter than the point-spread function (PSF) profile of the same star when the telescope is in sidereal mode. This is because the same photon flux is spread over multiple pixels in the image. As a result, many stellar traces of the faintest stars are lost below the noise level in the image background.

In StarView, we do not analyse the individual stellar traces in order to calibrate the satellite image. Instead, the calibration is performed using the two-dimensional cross-correlation technique to compute the exact equatorial coordinates of the image centre. In this way, all stellar traces found in the image are used simultaneously, significantly increasing the reliability of the calibration. This process is illustrated in Fig. 2. For a given satellite image, a simulated stellar frame is first constructed from the catalogue stars in the same sky region, as determined by the approximate equatorial position of the telescope (this information is available from the telescope control software and is stored in the image FITS header). In order to generate a simulated stellar image, the initial astrometric solution obtained from a reference stellar frame, as described above, is used. The only parameter that is changed is the equatorial position of the image centre. As a result, the simulated image contains the same stars that

were captured in the satellite frame, i.e. each stellar trace corresponds to a single star in the simulated frame. The only remaining task is to cross-correlate the satellite image with the simulated stellar image in order to determine the offset in pixel coordinates. This offset can then be converted to the corresponding angular coordinates in the sky, using again the initial astrometric solution.

The two-dimensional cross-correlation in StarView is obtained from a complex product of fast Fourier transforms (FFT) of the input images. We use a publicly available library [8] called The Fastest Fourier Transform in the West (FFTW). The cross-correlation image (Fig. 3) contains multiple traces (cross-correlation peaks) of the same shape and size as the original stellar traces in the satellite image. The strongest trace corresponds to the best alignment between the two images. When plotted in three dimensions, the cross-correlation maximum shows a complex variation of the pixel intensity. This is basically a reflection of the similar variation along a stellar trace in the satellite image, caused by the atmospheric turbulence (scintillation).

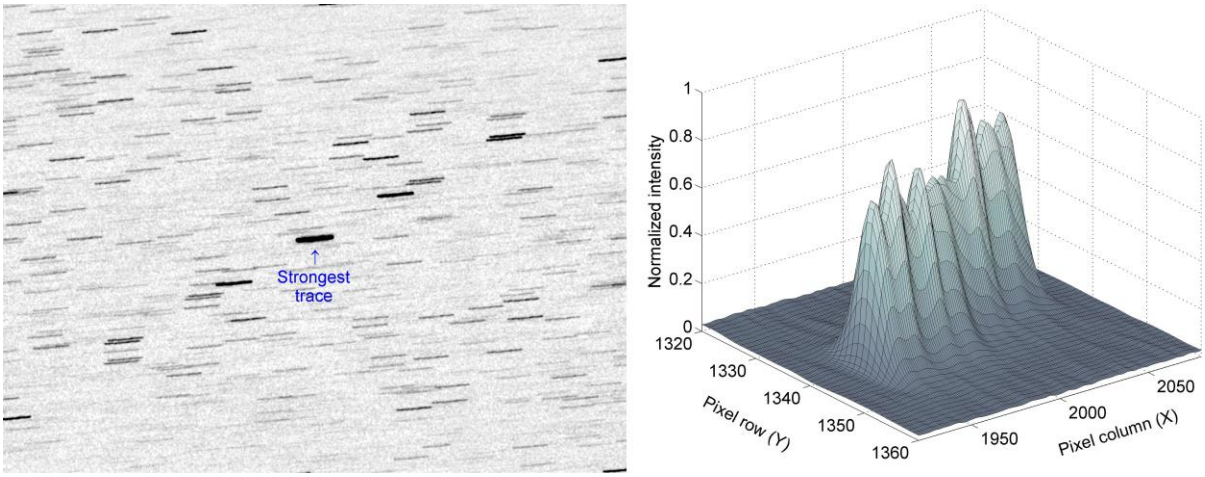

Fig. 3. Left: A typical cross-correlation image. Right: The intensity profile of the strongest trace.

Once the strongest trace has been identified, a special algorithm is used to analyse the shape of the intensity profile, as shown in Fig. 4. The algorithm has two main steps:

1. Initially, the profile ridge is traced by centring the cross-section of the profile at every pixel column. The simplest way to do this is to fit a Gaussian function to the core of the profile. When all the centres are found along the trace, a straight line is fitted to represent a smooth path in X and Y for the duration of the exposure.
2. Using the tracing data from the previous step, the pixel intensity is then integrated over the ridge profile at every pixel column. As a result, a flux profile is obtained, as shown in the right panel of Fig. 4. By analysing the rising edge of the profile, the X-coordinate corresponding to the start of exposure is obtained (when the flux profile reaches 50 per cent of the maximum intensity). Similarly, the end of exposure is determined from the falling edge when the profile drops to 50 per cent of the maximum intensity. The middle of exposure is found half-way between the edge points. Finally, to calculate the Y-coordinate of the profile centre, we use the linear fit to the cross-correlation trace obtained from Step 1.

With the X and Y pixel coordinates of the cross-correlation peak obtained above, we proceed to determine the shift between the observed satellite image and simulated stellar frame, where zero shift corresponds to the centre of the cross-correlation image. The shift in pixel units is then converted to an offset in right ascension and declination (using the calibration data from the reference stellar image), which is then applied to the astrometric measurement of the satellite.

An example of a measurement sequence is shown in Fig. 5. The observations are of TDRS 10, taken on the night of 4 August 2022, and cover a period of about 18 minutes (a total of 51 data points). The left-hand panels show the observed astrometric right ascension and declination. At this scale, the measurements look perfectly smooth, as the overall change in both coordinates is much larger than the measurement uncertainty. In order to examine the random

measurement errors, a low order polynomial was fitted to the data, and the residuals were plotted in the right-hand panels. The residuals in both coordinates are within a small fraction of an arc second, or about one third of an image pixel (taking into account the typical scale of 0.66 arc seconds per pixel).

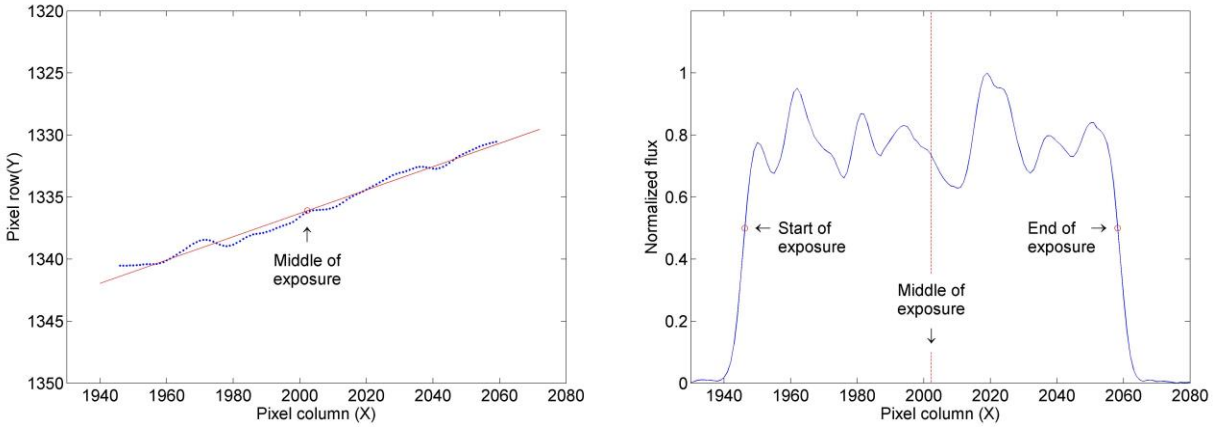

Fig. 4. Left: A linear fit to the central ridge of the cross-correlation trace. Right: Normalized flux along the ridge.

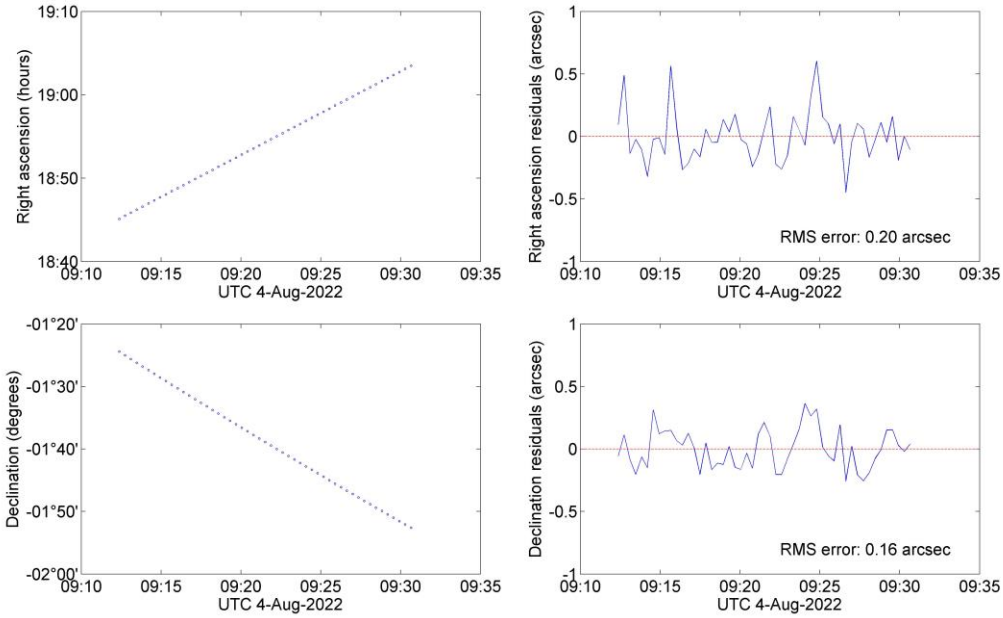

Fig. 5. Left: Observed astrometric coordinates of TDRS 10. Right: Residuals after a polynomial fit.

The random errors usually get larger with longer observation sequences due to a number of factors including any temperature variations inside the observatory, refocusing of the telescope, or flexure of the optical tube. Sometimes, an occasional measurement may fall well outside of the smooth polynomial fit, usually if the automated data reduction procedure fails (e.g. if the image is corrupted in any way, a very bright star enters the field of view, or a bright satellite trace crosses the frame). Only a small percentage of observations (typically, less than 5%) will fall into this category, and they can safely be rejected from the observation sequence.

3.3 Measurement accuracy

The analysis of the precision of the observations (random measurement errors) described above does not give us a measure of the accuracy of the final astrometric coordinates. In order to check the accuracy of astrometric

measurements, the data need to be compared with a reference ephemeris for the given satellite. One option would be to send the data to the 18 SDS, which must be done in a standard observation transmission format called B3 [9]. This is not our preferred option, for two reasons. Firstly, our measurements are essentially *astrometric* coordinates expressed in the International Celestial Reference System (ICRS), as defined by the GAIA catalogue used for the astrometric calibration. The B3 format, on the other hand, expects the *topocentric* positions that would take into account the fact that the observations were made from a location that moves with respect to the inertial reference frame. This requires additional reduction steps in our procedure. Secondly, the B3 format does not have the capacity to hold the full precision of our measurements. The right ascension in B3 can only be specified down to 0.1 s (1.5 arcsec), and the declination down to 0.0001 degrees (0.36 arcsec). This is significantly larger than our precision of 0.2 arcsec in right ascension and 0.16 arcsec in declination shown above.

We prefer to check our measurement accuracy directly at the level of astrometric coordinates using the reference ephemeris data that can be obtained on request from the 18 SDS. The ephemeris data are in a form of geocentric state vectors $(X, Y, Z, \dot{X}, \dot{Y}, \dot{Z})$ in the Earth-centered Earth-fixed (ECEF), also known as Earth-centred rotational (ECR), coordinate system. The data are tabulated at 10-minute intervals and need to be interpolated for the time of observation. A standard Lagrange polynomial interpolation is used in our data reduction procedure. The Cartesian coordinates obtained from the ephemeris file need to be converted to the astrometric equatorial coordinates for the exact geographic location of the sensor in order to be compared with the observations. We use the Standards of Fundamental Astronomy (SOFA) library [10] for this task. The main computational steps are:

1. Rotating the reference frame from terrestrial to celestial (ECEF to ICRS), which takes into account the polar motion, Earth's rotation angle, precession of the equinoxes and nutation of the polar axis.
2. Applying the light-time correction to account for the finite speed of light, as the observed direction to the satellite always corresponds to an earlier position in the orbit when the sunlight was reflected from the surface of the satellite.
3. Converting the Cartesian coordinates to the astrometric right ascension and declination for the time of observation.

4. RESULTS

The final results of our measurements are shown in Figures 6 – 8, where the residuals in right ascension and declination (i.e. the measured coordinates minus the ephemeris positions) are plotted as a function of the time of observation. The data show very low scatter of about 0.2 – 0.3 arc seconds, or less, which is in agreement with the random measurement errors. Also, there is no sign of a significant offset in the measurements, as the data mean in both coordinates stays mainly below 0.2 arc seconds. In other words, the data follow the predicted coordinates very well, and there is no statistical evidence that our astrometric measurements differ from the ephemeris positions.

A closer inspection of the charts reveals a possible weak trend in the slope of the residuals, mainly in declination, especially during the first hour of observation (e.g. on 3rd August). This might be caused, for example, by the gradual cooling of the equipment if the observations were started too soon after the observatory dome was open. However, more work would be required to test the statistical significance of any small effects like this, which was out of scope of this paper.

The results of this work demonstrate that inexpensive small-aperture optical equipment can be successfully used for accurate measurements of the position of a satellite in Earth's orbit. High-quality astrometric measurements of this level can provide a valuable input to a range of astrodynamics applications, such as orbit determination, manoeuvre detection and perturbation analysis.

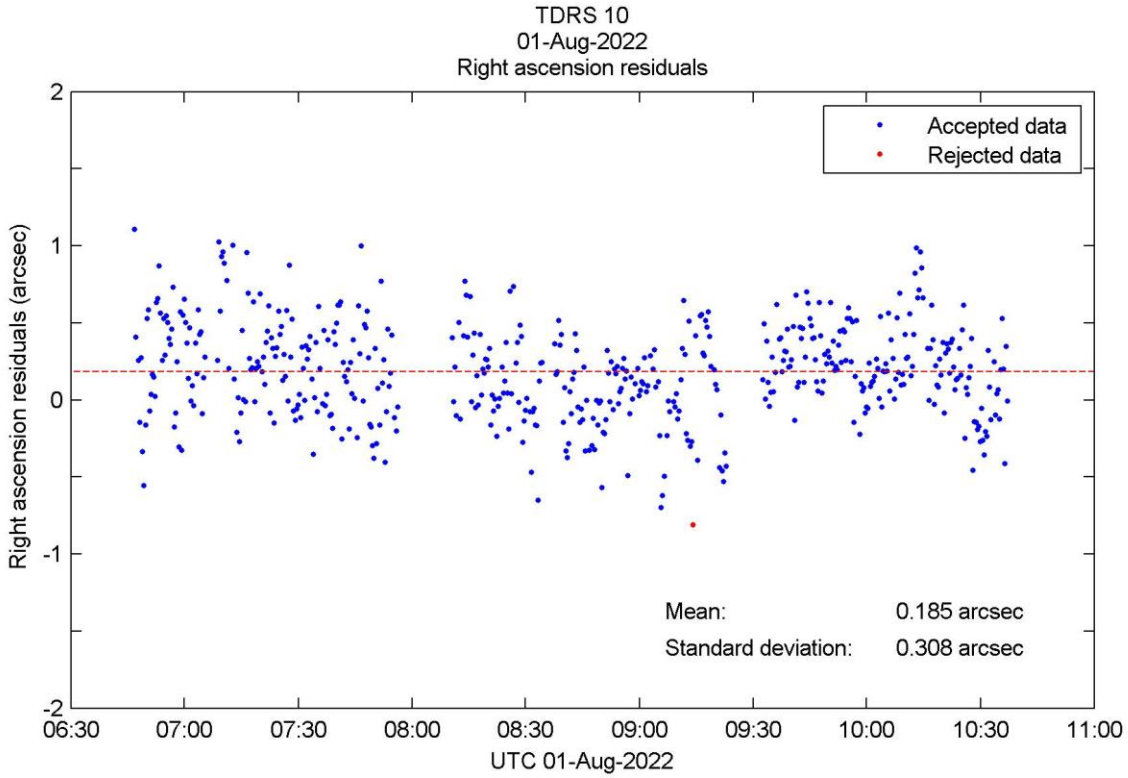

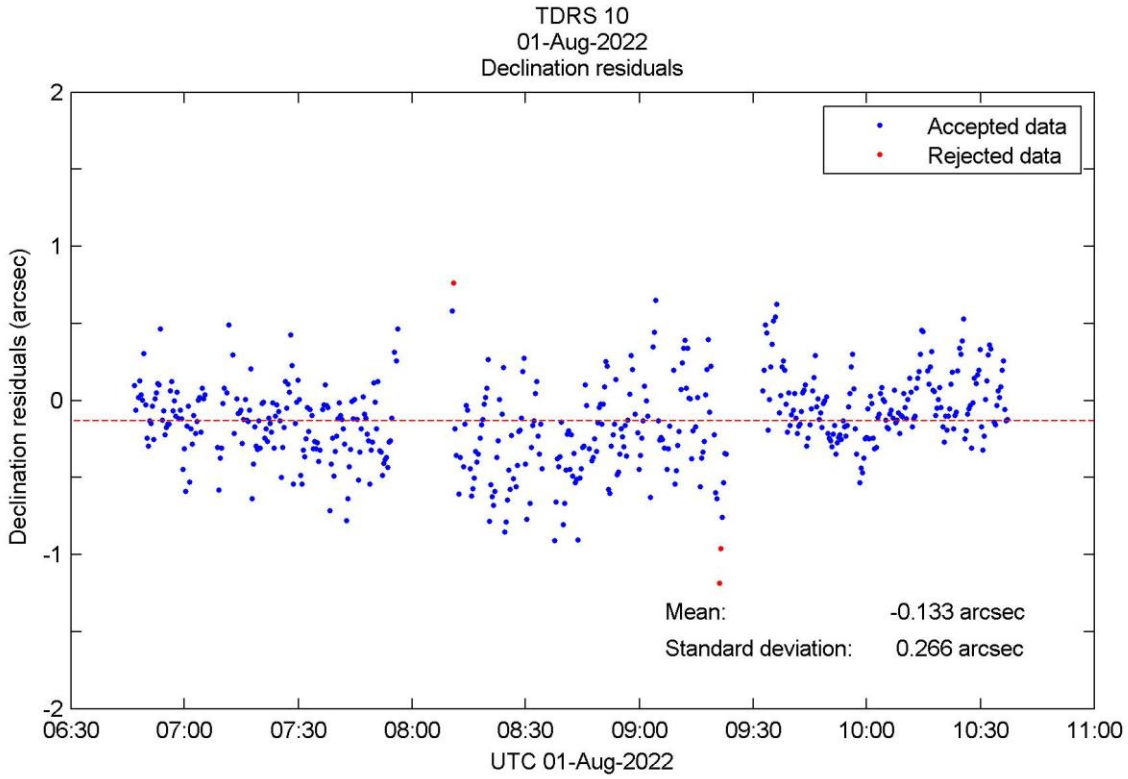

Fig. 6. Observations of TDRS 10 on 1 August 2022

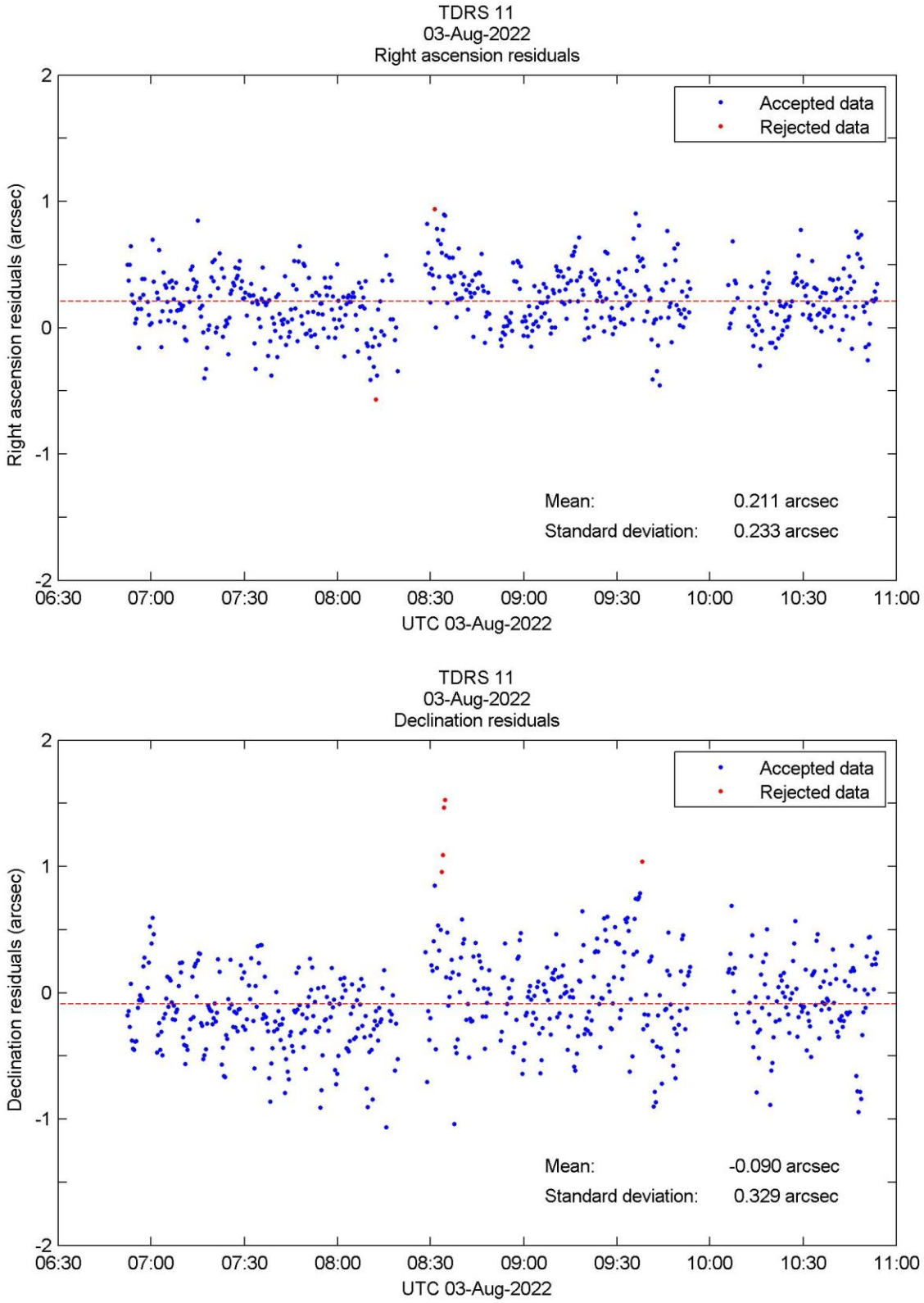

Fig. 7. Observations of TDRS 11 on 3 August 2022

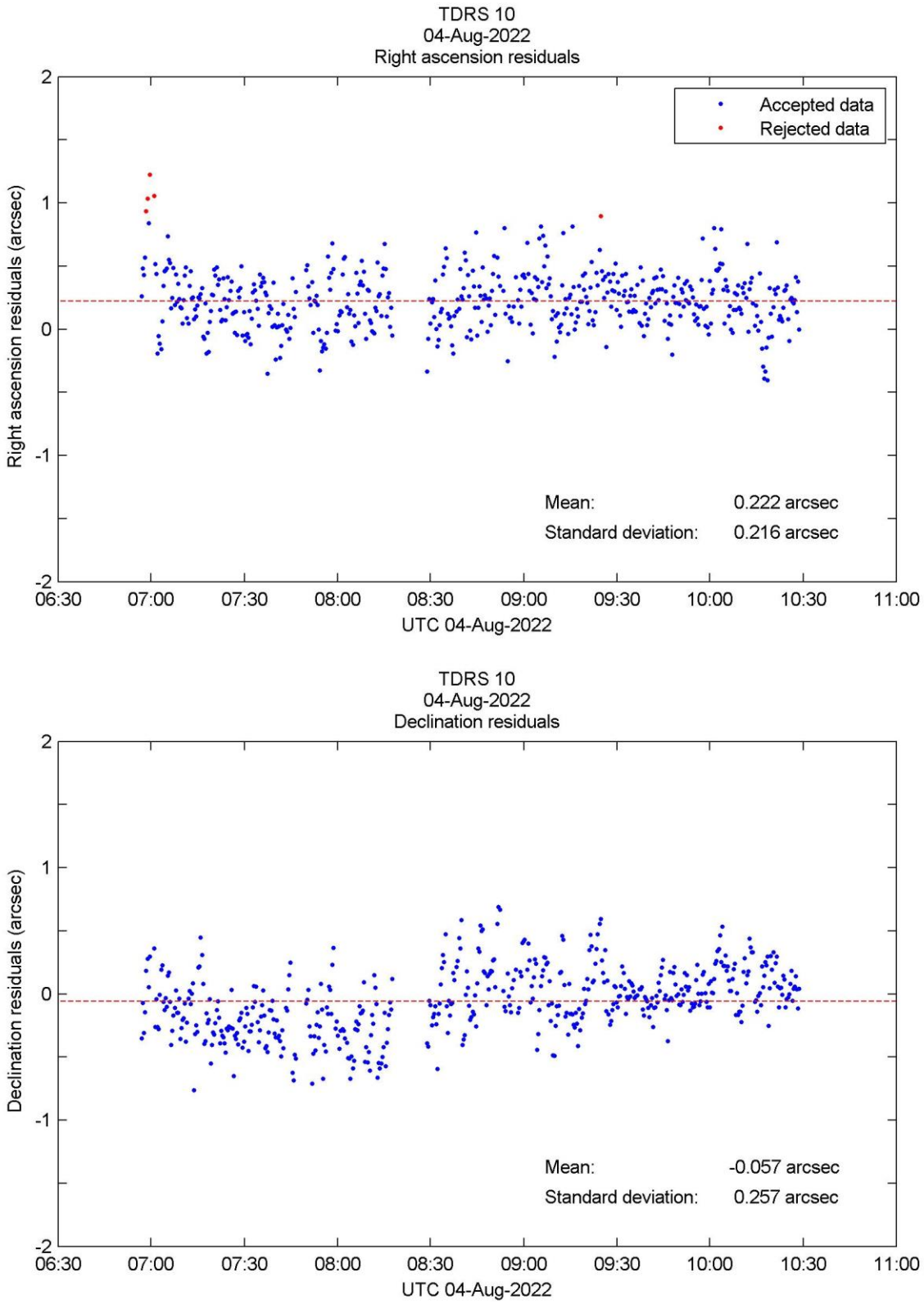

Fig. 8. Observations of TDRS 10 on 4 August 2022

5. REFERENCES

[1] J. Skuljan. Photometric measurements of geostationary satellites over the Western Pacific Region, *Proc. 19th AMOS Conf.,* pp. 1420-1428, 2018

[2] S. George, A. Ash. T. Bessell, L. Scott, J. Skuljan, J. Frith, R. Furfaro, V. Reddy. Phantom Echoes: A Five-Eyes SDA Experiment to Examine GEO Rendezvous and Proximity, *Proc 21st AMOS Conf.,* 97-114, 2020

[3] S. George, A. Agathanggelou, G. Privett, P. Halpin, W. Feline, A. Ash, L. Scott, J. Skuljan, J. Frith, J. Alvino, P. Chote. Phantom Echoes 2: A Five-Eyes SDA Experiment on GEO Proximity Operations, *Proc 22nd AMOS Conf.,* 2021

[4] J. Skuljan. Astrometric and photometric measurements of GEO satellites in proximity operations over the Pacific, *Proc 21st AMOS Conf.,* 1374-1383, 2020

[5] J. Skuljan and J. Kay. Automated astrometric analysis of satellite observations using wide-field imaging, *Proc. 17th AMOS Conf.,* 2016, 240-249

[6] Gaia Collaboration, Prusti, T., de Bruijne, J. H. J., Brown, A. G. A., Vallenari, A., Babusiaux, C., Bailer-Jones, C. A. L., Bastian, U., Biermann, M., Evans, D. W., et al., The Gaia mission, *A&A,* 595, pp. A1, 2016

[7] F. van Leeuwen, E. Fantino. A new reduction of the raw Hipparcos data, *Astron. Astrophys.* 439, 791-803, 2005.

[8] M. Frigo, S. G. Johnson. The fastest Fourier transform in the West, Manual for version 3.3.3., 2012 (http://www.fftw.org)

[9] Air Force Space Command Astrodynamic Standards, AFSPC Instruction 60-102, 11 March 1996

[10] SOFA - International Astronomical Union Standards of Fundamental Astronomy (http://www.iausofa.org)